Applied Surface Science 606 (2022) 154880

Contents lists available at ScienceDirect

Applied Surface Science

journal homepage: www.elsevier.com/locate/apsusc

Full length article

Unraveling the mechanism to form MoS_2 lubricant layers from MoDTC by ab initio simulations

Stefan Peeters [a], Gabriele Losi [a], Paolo Restuccia [a,b], M.C. Righi [a,c,*]

[a] Department of Physics and Astronomy, University of Bologna, Viale Carlo Berti Pichat 6/2, Bologna, 40127, Italy
[b] Department of Chemistry, Imperial College London, 82 Wood Lane, London, W12 0BZ, UK
[c] Department Mechanical Engineering, Imperial College London, South Kensington Campus, London, SW7 2AZ, UK

ARTICLE INFO

Keywords:
Crystallization
MoS_2
MoDTC
Tribochemistry
Ab initio molecular dynamics
Lubricants

ABSTRACT

The morphology of molybdenum disulfide (MoS_2) is a crucial aspect to ensure the functionality of this remarkable 2D-material both in electronic and tribological applications. Indeed, molybdenum dithiocarbamates (MoDTCs) can be tribochemically transformed into MoS_2, which is able to reduce the friction coefficient of metallic moving parts. However, this transformation is influenced by temperature, sulfur/oxygen ratio, normal and shear stresses, making the mechanism of this process particularly challenging to explain. Ab initio simulations based on density functional theory (DFT), including a quantum mechanics/molecular mechanics (QM/MM) approach, are used here to shed light on the crystallization of MoS_2 promoted by mechanical stresses. Chemistry plays an important role during the reorganization of the units of MoS_x obtained from MoDTC, because sulfur and oxygen atoms tend to move outside of the amorphous layer, surrounding the molybdenum atoms and creating a structure that can crystallize into MoS_2. Normal load and sliding have a synergistic effect in rearranging the amorphous units into a crystalline structure, as the former helps overcoming the energy barriers associated to bonds breaking and forming, while the latter allows misplaced atoms to be pulled towards the crystalline sites. A crystalline MoS_2 was obtained by ab initio calculations below 1000 K.

1. Introduction

Molybdenum disulfide (MoS_2) is a fascinating layered material because of its remarkable properties. This transition metal dichalcogenide (TMD) is employed as a catalyst in several photoelectrochemical [1–3] and optoelectronic applications [4,5]. For all these different purposes, the morphology of the MoS_2 layers is a crucial factor to ensure the proper performance of the devices. Indeed, the synthesis of MoS_2 requires precise conditions to achieve the desired size of the crystals, thickness and the density of defects [6].

MoS_2 is also successfully employed as a solid lubricant, because its weak interlayer forces offer very little resistance to sliding and prevent the formation of interfacial bonds in moving parts [7–9]. High cristallinity of MoS_2 is beneficial in tribological applications, because the repulsive interlayer interactions are maximized in crystalline layers [10]. Several authors investigated the crystallization of MoS_2 by *in-situ* experimental techniques and identified the existence of different polymorphs during the formation of the film [6] and described the effect of the substrate [11] and temperature [12–15] during the transformation. However, *in-situ* techniques are often limited by the difficulty of monitoring the full crystallization at high temperatures.

Simulations are particularly useful to investigate the debated aspects of this complicated reactivity. Nicolini et al. studied the reaction parameters and the conditions to obtain a crystalline MoS_2 layer by means of reactive molecular dynamics [16]. They have very recently proposed a new parametrization for a reactive force field that provides results closer to the predictions by density functional theory [17]. Chen et al. also simulated the crystallization of MoS_2 by using different reactive force fields and took into account the effect of oxygen in hindering the transformation [18]. Reactive force fields such as the Adaptive Intermolecular Reactive Empirical Bond Order (AIREBO) [19] and ReaxFF [20] can often model the formation and breaking of chemical bonds. However, these force fields were not originally designed to reproduce the chemical properties of the species under the effect of confinement and stresses that can be typically observed in tribological applications. Therefore, ab initio approaches are better suited to describe the changes in the electronic structure due to such extreme conditions [21].

In automotive applications, the precursors of MoS_2 are molybdenum dithiocarbamates (MoDTCs), a group of organo-molybdenum lubricant

* Corresponding author at: Department of Physics and Astronomy, University of Bologna, Viale Carlo Berti Pichat 6/2, Bologna, 40127, Italy.
E-mail address: clelia.righi@unibo.it (M.C. Righi).

https://doi.org/10.1016/j.apsusc.2022.154880
Received 15 June 2022; Received in revised form 30 August 2022; Accepted 9 September 2022
Available online 14 September 2022

additives which can be transformed into MoS_2 in the presence of high temperatures and mechanical stresses. The mechanism underlying the transformation of MoDTC in MoS_2 is a complex series of tribochemical steps that have been the subject of debate in the last years [22,23]. Sulfur and oxygen present at the interface play an important role in this reaction: MoDTC compounds undergo quick oxidation in air, causing the chemical structure and properties of these complexes to change [24], while the synergy of MoDTC with zinc dithiophosphates (ZnDTP), common anti-wear additives, is capable of replenishing the sulfur atoms lost by oxidation [25–27]. In our recent works, we described the complex chemistry of these compounds. We first studied the properties of isolated MoDTC compounds and identified the ligand position, between Mo and C, as the most favorable site for oxygen in the molecules [28]. Indeed, the ratio between sulfur and oxygen and the position of these atoms in the complex influence their reactivity on the metallic surface. MoDTC with oxygen in ligand position is able to generate small clusters containing Mo and S atoms with the correct stoichiometry to form MoS_2 [29], while this phenomenon was not observed in our simulations for MoDTC compounds with oxygen in the terminal position, on top of Mo. Oxygen can also hinder the transformation of the complexes into MoS_2, when passivating the metallic surface. MoDTC is not fully able to chemisorb and decompose on passivated surfaces and some time is required to remove the oxide layer in excess, giving rise to the run-in period typically observed experimentally [30]. Furthermore, mononuclear MoDTC can also play a role in forming MoS_2 and we showed that an equilibrium between the mononuclear and the more conventional binuclear forms of MoDTC is possible [31]. In these recent studies, we focused our investigation on the formation of fragments from the central core of MoDTC, containing Mo, S and O atoms. These units, that can vary by their size and composition, can be collectively referred to as MoS_x [32,33]. The aim of this work is to complete the description of the tribochemical reaction from MoDTC to the tribofilm by focusing on the conversion of different units of MoS_x into a crystalline MoS_2 layer, which is the remaining step to be clarified. We employed density functional theory (DFT) to simulate the tribochemical transformation of the units of MoS_x to form crystalline MoS_2 in different steps. Firstly, we performed static calculations of MoS_x units under load to monitor how compression can destabilize the geometry of these molecular fragments. Dynamic calculations, following the scheme of quantum mechanics/molecular mechanics (QM/MM) [34,35], were then performed to introduce the effect of temperature and shear stress on the destabilized MoS_x units. The QM/MM computational approach was chosen because it is a very convenient technique in tribochemistry to describe reactions with the desired chemical accuracy while keeping the simulations computationally affordable [29,30,36]. We also explored the role of oxygen in the MoS_x units, as it is known that the presence of oxygen does not necessarily prevent the formation of MoS_2 layers [33], yet O atoms modify the morphology and composition of the layers of this solid lubricant [37]. Lastly, we simulated the crystallization of an amorphous layer containing Mo and S atoms by means of Car–Parrinello dynamic simulations [38], which do not require the use of empirically-parametrized force fields, making this work the first ab initio investigation, to the best of our knowledge, concerning the final steps of the transformation of MoDTC into MoS_2. This computational approach allowed an in-depth understanding of the effect of stresses, temperature and the role of oxygen in the rearrangement of fragments of MoDTC into crystalline MoS_2, overcoming the challenges faced by experimental techniques and reactive force fields.

2. Methods and systems

The ab initio calculations were carried out by employing the Quantum ESPRESSO computational suite [39], following the pseudopotentials/plane waves scheme. For all the calculations the Perdew–Burke–Ernzerhof (PBE) approximation [40] was used for the exchange–correlation functional. The plane waves expansion was limited by cutoffs equal to 30 and 240 Ry for the kinetic energy and the charge density, respectively. The pseudopotential were ultrasoft and all the integrations were carried out at the Γ point. Spin polarization was considered to allow spin multiplicities higher than singlets. In order to better describe the occupations of the electronic states around the Fermi level, a Gaussian smearing of 0.02 Ry was added. The self-consistent field calculations were stopped when the change on the total energy was lower than 1×10^{-6} Ry, while the geometry optimizations were stopped when the total energies and the forces on the atoms converged below the thresholds of 1×10^{-4} Ry and 1×10^{-3} Ry/bohr, respectively. The specific details for the two sets of simulations, namely the QM/MM simulations for the reorganization of the fragments of MoDTC and the Car–Parrinello simulations for the crystallization of MoS_2, are reported in the following sections.

2.1. Reorganization of the central units of MoDTC

Twelve units of MoS_x, originated from the central core of MoDTC and enclosed by two crystalline MoS_2 layers, were put inside a periodic $5 \times 3\sqrt{3}$ cell with respect to the unit cell of MoS_2, with the cell dimensions being 16.62×15.99×33.59, expressed in Å. Such a cell height ensured at least 15 Å of vacuum to separate the periodic replicas. Even though the formation of MoS_2 tribofilm is often observed on metallic substrates, crystalline MoS_2 layers were chosen as the external layers instead, because using the target structure as external layer can help the reorganization of the inner species due to the commensurability its lattice, while other materials can hinder the process due to the lattice mismatch. Furthermore, we are interested in describing the tribofilm formation after the initial passivation of the metallic surface, when the tribofilm grows through the reorganization of MoS_x. In this case, the central units of MoDTC may adsorb and rearrange on top of other MoS_x structures, or even crystalline MoS_2.

Two different kinds of MoS_x units were considered: units containing only molybdenum and sulfur were assigned to one group of simulations, while units with two oxygen atoms in terminal position were also taken into account. To simulate a compressive stress on the MoS_x units, external forces were imposed on the molybdenum atoms of the crystalline MoS_2 layers. The initial load experienced by the central units was 10 GPa. After the first geometry optimization, the load was increased to 20 and then 40 GPa.

To introduce the effect of shear on the compressed units, we carried out dynamic calculations following the QM/MM approach already described in detail in our previous publication [29]. This computational approach allows to compute the total energy of the system by a subtractive scheme [41]:

$$E_{tot} = E^{\mathrm{I+II}}_{\mathrm{MM}} - E^{\mathrm{I}}_{\mathrm{MM}} + E^{\mathrm{I}}_{\mathrm{QM}} \quad (1)$$

where E_{tot} is the total energy of the whole QM/MM system, $E^{\mathrm{I+II}}_{\mathrm{MM}}$ is the total energy of the whole system computed with the classical force fields, while $E^{\mathrm{I}}_{\mathrm{MM}}$ and $E^{\mathrm{I}}_{\mathrm{QM}}$ are the total energies of the reactive region, computed classically and at the quantum level, respectively. The calculations at the quantum level were carried out by Quantum ESPRESSO, while the overall dynamics was handled by the LAMMPS software [42]. Three QM/MM simulations were carried out depending on the type of MoS_x units in the system and their interaction with the external crystalline layers:

- System A: MoS_x units containing only Mo and S atoms. The simulation time is 10 ps
- System B: MoS_x units containing also O atoms. The interactions between the oxygen atoms and the external MoS_2 layers were described by an attractive Lennard-Jones potential. The simulation time is 10 ps
- System C: MoS_x units containing also O atoms. The interactions between the oxygen atoms and the external MoS_2 layers were described by a repulsive Lennard-Jones potential. The simulation time is 8 ps

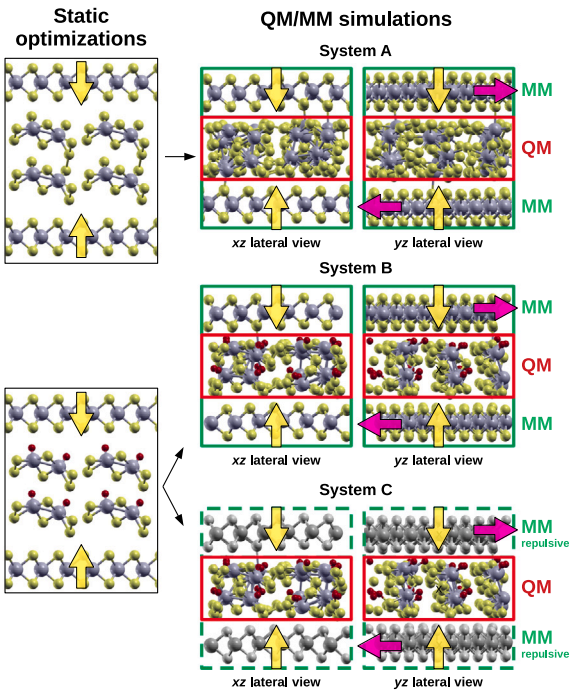

Fig. 1. Lateral views of the initial configurations of the systems containing the MoS_x units. Yellow and purple arrows in the figure identify load and shear, respectively. Red, yellow and gray spheres correspond to oxygen, sulfur and molybdenum atoms, respectively. System A contains MoS_x units with only molybdenum and sulfur, while Systems B and C also include oxygen. In System B (C), the O atoms are attracted to (repelled by) the external two layers, as explained in the main text.

The parameters chosen for the attractive and the repulsive Lennard-Jones potentials are described in Appendix. Selecting different potentials to describe the interactions of O atoms with the external layers in Systems B and C allowed to investigate the behavior of the oxygen in two different environments and to describe the diffusion of the O atoms in the central layer independently of the chemistry of the external layers. The interactions between the Mo and S atoms of the MoS_x units and the external MoS_2 layers were described by the REBO-MoS_2 potential by Liang et al. [43,44] in all the systems. An initial thermalization process, lasted one picosecond, allowed the system to globally reach 300 K by employing a Nosé–Hoover thermostat with a damping parameter of 33.3 fs. An ensemble of velocities for all the atoms was generated from a Gaussian distribution with a standard deviation scaled to produce the temperature of 300 K. After the thermalization process, the temperature of the chemically reactive region was left free to evolve and, in order to simulate the sliding of the surfaces, velocity kicks were applied on the Mo atoms of the external layers every picosecond. Initially, 600 m/s were applied at the first and second picosecond. Since the sliding motion of the external layers stopped due to their strong interaction with the inner layers, the kicks were increased to 800 m/s at the third and fourth picosecond, and to 1000 m/s from the fifth picosecond onwards. Such high values of shear speed were necessary to counteract the high friction induced by the very high load, and they never exceeded the speed of sound in MoS_2, being approximately 7900 m/s [45]. The timestep of the simulation was 1 fs. The MoS_x units experienced a load of 40 GPa for the whole duration of the simulation. A schematic representation of these systems is shown in Fig. 1.

2.2. Crystallization of the amorphous MoS_x layer

In order to simulate the crystallization of MoS_2 from an amorphous layer, we employed a modified version of the Car–Parrinello solver of Quantum ESPRESSO created by our group to simulate properly tribological systems [46]. The system is composed of an amorphous layer of MoS_2, enclosed by two crystalline MoS_2 layers in a periodic $5 \times 3\sqrt{3}$ cell. The choice of the simulation cell dimensions, pseudopotentials, K-points sampling, kinetic energy and charge density cutoffs were the same as the one used for the previous QM/MM calculations. However, the geometry of the amorphous layer containing only Mo and S atoms was generated specifically for this set of simulations, as the stoichiometry of the structures obtained previously would not match the one of crystalline MoS_2. The amorphous layer was generated in the same $5 \times 3\sqrt{3}$ cell through classical molecular dynamics simulation using the LAMMPS package and employing the REBO-MoS_2 force field described in the previous section. To obtain the amorphous layer, we followed a similar procedure as described in Ref. [16]: we heated up a MoS_2 layer at 5500 K for 100 ps using a chain of Nosé–Hoover thermostat with a damping factor of 10 fs in order to melt the monolayer. Then, we quenched the system to 300 K in 15 ps in order to create the amorphous structure.

After the generation of the amorphous structure, we initially thermalized the system with a Nosé–Hoover thermostat with a frequency of 200 THz on the ions and on the electrons, in order to reach an average kinetic energy of 0.2 hartree. The fictitious electronic mass was 450 a.u. and the time step was 5 a.u., corresponding to 0.12 fs. Grimme's DFT-D2 correction was included in these calculations to better describe interlayer interactions [47]. A lateral shear and a load were applied on the external layers, similarly to the QM/MM simulations. A set of different dynamic simulations were performed depending on the external stresses and temperature imposed on the system. The details of all the simulations are presented in Table 1, while the initial geometry and a scheme summarizing the dynamic simulations are shown in Fig. 2.

3. Results and discussion

3.1. From MoS_x units into an amorphous layer

Normal load destabilized the molecular units, which immediately rearranged their geometry in the static calculations. After reaching 40 GPa, the original geometry of the MoS_x units is lost, yet the Mo atoms are still clustered in the same locations where the units were initially positioned. To allow further reorganization, the optimized configurations at 40 GPa were chosen as the initial geometry of the

Table 1
Conditions of the Car–Parrinello molecular dynamics simulations of the crystallization of MoS_2.

Simulation	Load (GPa)	Shear force (nN/layer)	Temperature (K)	Total time (ps)
1	1.4 (until 11 ps) 2.8 (from 11 ps)	1.33	600	26.1
2	1.4 (until 11 ps) 2.8 (11–13.5 ps) 5.6 (from 13.5 ps)	1.33 (until 19.5 ps) 5.32 (from 19.5 ps)	600 (until 33.6 ps) 900 (from 33.6 ps)	46.9
3	1.4 (until 11 ps) 0.28 (11–13.4 ps) 2.8 (13.4–15.8 ps) 0.28 (15.8–18.2 ps) 2.8 (18.2–20.6 ps) 0.28 (20.6–23 ps) 2.8 (from 23 ps)	1.33 (until 11 ps) 2.66 (from 11 ps)	600	25.5
4	1.4	1.33	600	20.7
5	5.6	1.33	600	11.7
6	1.4	1.33	900	14.1
7	1.4	5.32	600	8.8
8	5.6	5.32	600	22.6
9	2.8	2.66	600	6.2

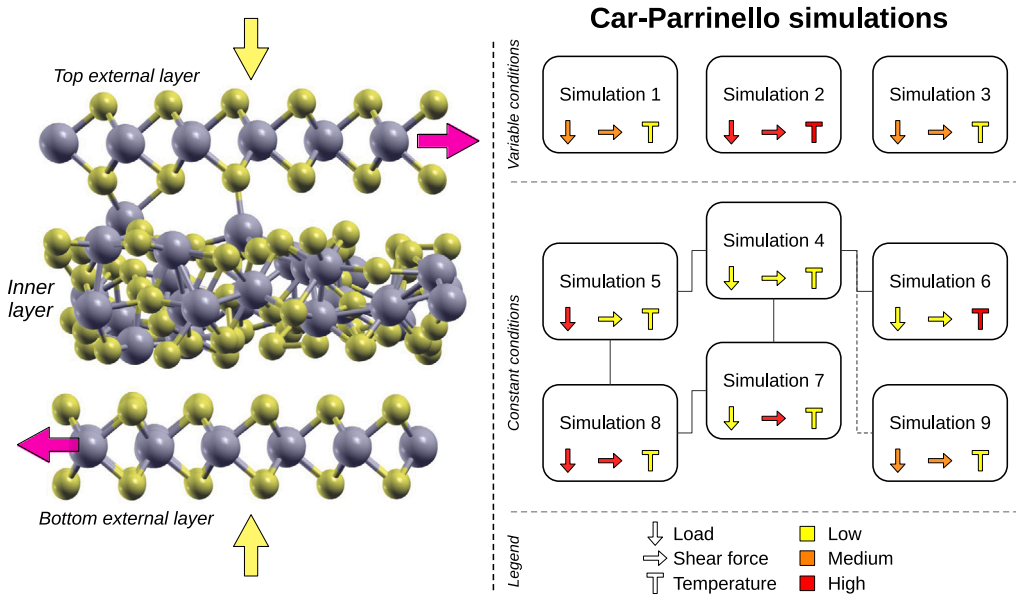

Fig. 2. Left: initial geometry of the Car–Parrinello dynamic simulations. Yellow and purple arrows identify load and shear, respectively, while yellow and gray spheres correspond to sulfur and molybdenum, respectively. Right: schematic representation of the simulations. The symbols of the simulations in the top row, in which the conditions vary, refer to load, shear force and temperature at the end of the simulations. The simulations connected by a solid line differ by one of the parameters, while Simulations 4 and 9, differing by two parameters, are connected by a dashed line. The conditions are explained in detail Table 1.

QM/MM dynamic simulations, in which the effect of temperature and the shear motion along the *y* direction were introduced. All the atoms from the MoS_x units were treated at the quantum level, while the atoms of the external MoS_2 layers were treated by means of classical molecular mechanics.

It is worth to compare the density of Mo, S and O atoms along the three axes at the beginning of the simulation and after 8 ps. The displacement of the atoms during the dynamic simulations changes the shape, the position and the height of the peaks of the density plots. This is particularly evident in the vertical direction, as shown in Fig. 3, where the Mo atoms tend to move towards the center of the inner layer in all the systems, while the density of S and O atoms increases at the edge of the inner layer. This phenomenon is an inherent feature of the inner layer, as pointed out by Krbal et al. in a recent study [48], and is mainly due to the tendency of Mo atoms to reach a high coordination. Oxygen always tends to reach the end of the inner layer, even when a repulsion is imposed between the external MoS_2 layers and the O atoms (System C). Furthermore, the presence of O atoms could influence the kinetics of the rearrangement of the MoS_x units. In System A, the distribution of the Mo atoms after 8 ps is similar to the initial one. Indeed, the peaks of the density plots became sharper for System A, indicating that the system reached a more organized state. In the case of Systems B and C, the structural change of the inner layer is more evident, suggesting that the rearrangement becomes quicker when oxygen is present. A possible reason for this effect could be due to the different commensurability of the inner layer with respect to the external layers depending on the presence of O atoms. The surfaces of the inner layer exposed to the external layers is more homogeneous, making the interaction between inner and external layers stronger and hindering the diffusion of the misplaced atoms. On the other hand, oxygen in the inner layer might play the role of a catalyst, as it may aid the rearrangement of Mo and S atoms, since the structure is less homogeneous and the effect of the mechanical stresses can be larger on the structural defects. Indeed, Krbal et al. have suggested that the growth of crystalline MoS_2 can occur even in the presence of incommensurate substrates.

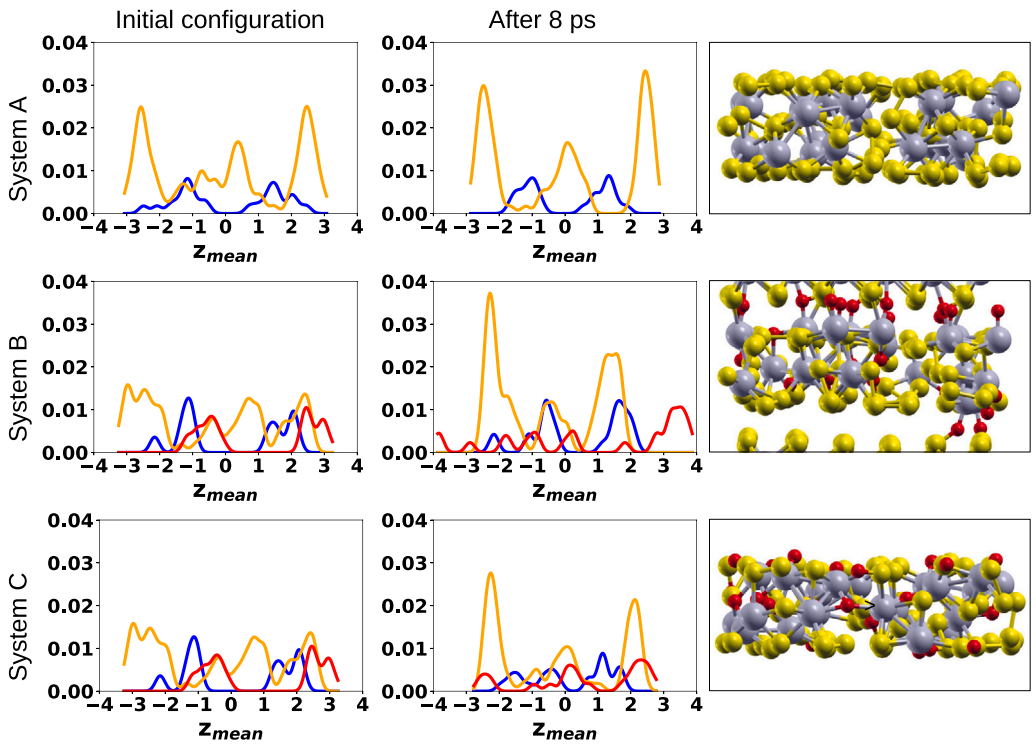

Fig. 3. Densities of O (red), S (yellow) and Mo (gray) atoms along the z axis of the cell during the QM/MM simulations. The rightmost panels show the geometries of the amorphous layers after 8 ps of dynamic simulation.

3.2. From the amorphous MoS_x layer to crystalline MoS_2

In the Car–Parrinello simulations 1–3, the temperature of the systems and the load and shear force imposed on the external MoS_2 varied. The change in temperature and mechanical stresses allowed to easily explore a wide range of different conditions. The most representative conditions were then investigated individually in Simulations 4–9, in which temperature and stresses were kept constant. The interlayer distance between the external crystalline MoS_2 layers and the final geometries of each system are shown in Figs. 4 and 5, respectively.

Simulations 1–3 shared the first 11 ps. In Simulations 1 and 2, the load was doubled after 11 ps, and in Simulation 2 the load reached four times its initial value at 13.5 ps. In both cases, the amorphous MoS_2 layer started rearranging immediately. The distribution of the atoms in the inner layer gradually became similar to the one of the external layers. However, the higher load in Simulation 2 drove a more pronounced rearrangement that made the inner layer commensurate with respect to the external layers. As in the case of the previous QM/MM simulations, the increase in commensurability comes with an increase in the interactions between the sliding external layers, causing a braking of the sliding motion. Indeed, at 19.5 ps the shear force was increased to four times the initial value, in order to recover the sliding motion, which helped further rearrangement of the Mo and S atoms. At approximately 30 ps the first crystalline unit of MoS_2, with one Mo atom surrounded by six S atoms, was observed in the inner layer and, since no significant evolution of the inner layer could be achieved in the following picoseconds, the temperature of the system was increased to 900 K at 33.6 ps. In the end, the inner layer could not completely become crystalline during the simulation, yet several crystalline clusters could be recognized, unlike in Simulation 1, where the reorganization was less complete. Simulation 3 was characterized by regular increases and decreases of the load once every 2.4 ps, in such a way that the external layers repeatedly pressed the inner layer. However, this solution was less efficient than the ones adopted in Simulations 1 and 2, as the amorphous layer underwent only a minor rearrangement.

Simulation 4 also shared the first 11 ps with Simulations 1–3, yet the same conditions were maintained throughout the whole run. Even though the cristallinity of the inner layer did not improve significantly, Simulation 4 represents an useful reference, as the conditions were the mildest compared to all the other systems. Simulations 5, 6 and 7 differed by a single condition from Simulation 4, namely a higher load, a higher temperature and a higher shear force, respectively. None of these simulations showed a significantly different inner layer from the one obtained in Simulation 4. In particular, the high load and low shear force in Simulation 5 caused the sliding motion to stop, hindering the diffusion of Mo and S atoms of the middle layer.

The inner MoS_2 layer became completely crystalline in Simulation 8, characterized by high load and shear force, and a temperature of 600 K. The system reached high cristallinity at around 9 ps, and the remaining vacancies were filled at 19 ps. Simulation 9, characterized by intermediate load and shear force between Simulation 4 and 8, also shows a mild reorganization of the inner layer, that will most probably end up in a crystalline layer at later times than the ones observed in Simulation 8.

One possibility to monitor the cristallinity of the inner MoS_2 layer is to calculate the total energy difference between a particular configuration of the layer E_{inner} and the average energy of the external layers $\langle E_{external} \rangle$ during the simulation:

$$\Delta E = \frac{1}{A}(E_{inner} - \frac{1}{2}\langle E_{external} \rangle) \quad (2)$$

where A is the area of the simulation cell. The values of ΔE calculated every 5.5 ps are reported in Fig. 6 for all the simulations, and clearly indicate that only in the case of Simulation 8 the energy difference between the inner and the external layers becomes negligible.

To better understand the mechanism behind the crystallization observed in Simulation 8, the coordination number of the Mo atoms in the system was taken into account. In Fig. 7, the Mo atoms of the system at different times are colored in blue, white or red when their coordination number is lower, equal or higher than 6, respectively. At the beginning of the simulation (Fig. 7, Panel a), most of the atoms of

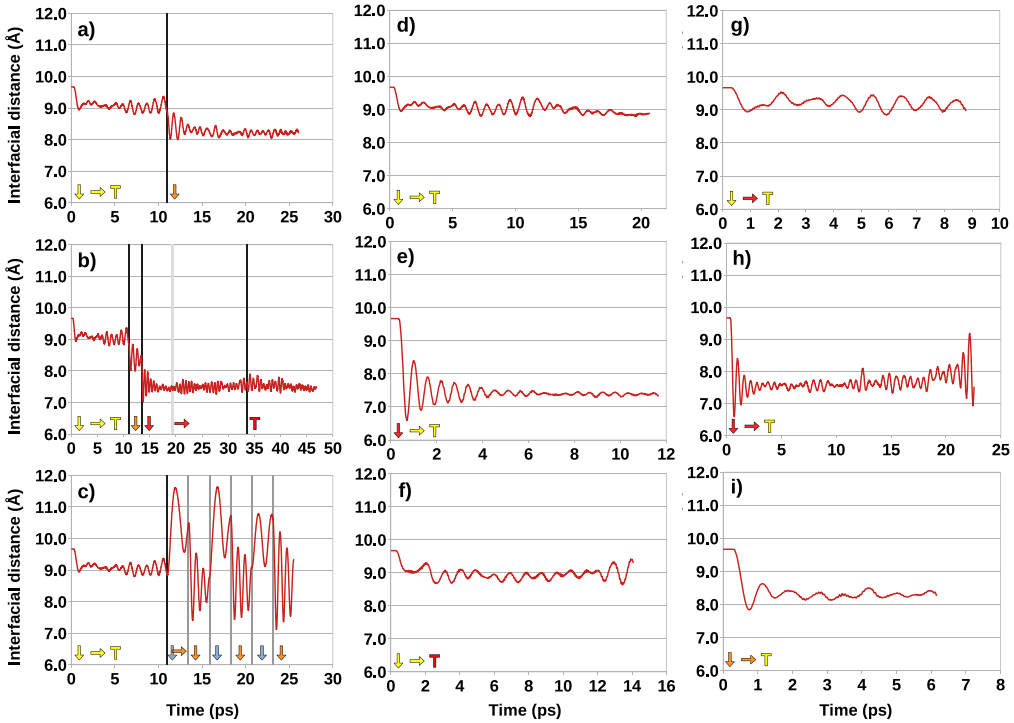

Fig. 4. Interfacial distance between the two crystalline MoS_2 layers in the dynamic simulations. Panels a–i correspond to Simulations 1–9, respectively. The symbols in the bottom left corner of each plot indicate the initial load, shear force and temperature of the simulation, in agreement with Fig. 2 and Table 1. Additional symbols in Simulations 1–3, appearing next to a vertical line, indicate a change in a specific condition. The light blue vertical arrows in Simulation 3 represent a load of 0.28 GPa.

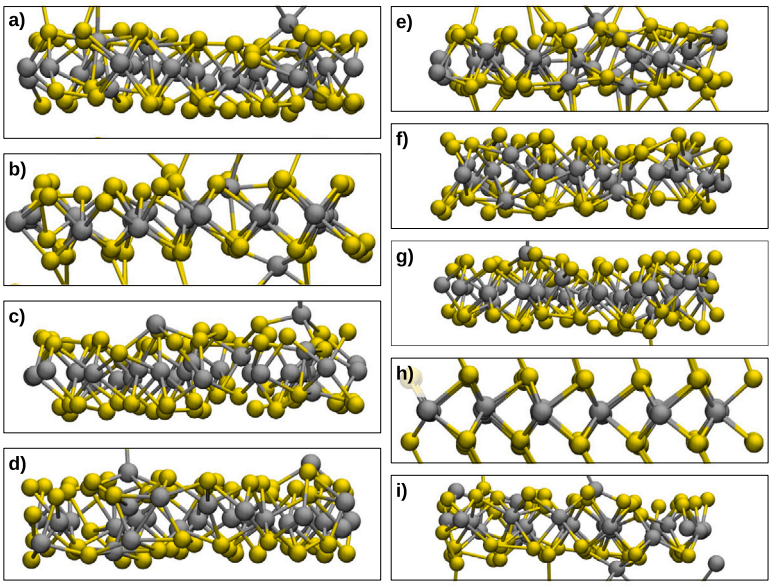

Fig. 5. Geometries of the inner MoS_2 layer at the end of the Car–Parrinello simulations. Panels a–i correspond to Simulations 1–9, respectively.

the inner layer were undercoordinated. While most of the Mo atoms underwent only a moderate rearrangement in the first picoseconds of the simulation, the S atoms quickly moved to the edge of the inner layer and started building the rows in the x and y directions observed in crystalline MoS_2. It has been shown experimentally that the energy barrier for the crystallization is mainly determined by the migration of the S atoms towards the surface of the layer [49,50]. Although we did not evaluate the energy barriers for atomic migrations in this study, this diffusion of the S atoms was observed in the first picoseconds of all our simulations, suggesting that the mechanical stresses promote the crystallization at lower temperatures compared to purely thermally-activated processes.

After 10 picoseconds (Panel b), several Mo atoms of the inner layer could be found at the correct height and were surrounded by 6 atoms. Under- and overcoordinated Mo atoms were still present, as the defects in the layer caused some of the Mo–S bonds to be strecthed or compressed. In this phase, some Mo atoms were far away from a crystalline site, and they were often pulled out from the inner layer, to be temporarily stabilized by the adjacent sulfur atoms of the external layers. Between 10–19 (Panel c) picoseconds, almost all of the atoms reached a

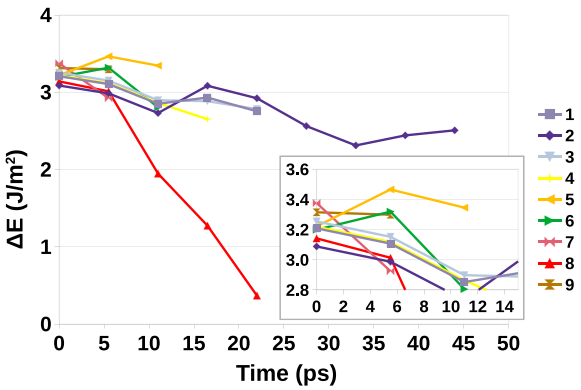

Fig. 6. Energy difference of the inner MoS_2 layer from the crystalline external layers for all the simulations.

crystalline site, while very few Mo were misplaced. Crystallization was achieved following the same mechanism: heavily misplaced Mo atoms are seized by one of the external layers and dragged until they find a vacancy, which is quickly filled. The resulting structure of the inner layer, namely the 2H phase of MoS_2, is indistinguishable from the one of the external layers (Panel d).

In their recent study, Krbal et al. were able to simulate the crystallization of the 1T' phase of MoS_2, corresponding to an intermediate state between the trigonal 2H structure and the octahedral 1T structure, after 200 ps at 1800 K by using density functional theory [48]. It is evident from our QM/MM and Car–Parrinello simulations that normal load and sliding have a synergistic effect in promoting the crystallization. In our case, mechanical stresses allowed to obtain the 2H phase of MoS_2 much earlier, and at a lower temperature. Several authors have shown that tribochemical reactions can be described by a stress-activated Arrhenius model [51–54]. Indeed, load allows to overcome energy barriers associated to the breaking and the formation of chemical bonds. By pushing atoms close together, the reactivity is enhanced due to electronic repulsion. Furthermore, the initial configuration shown in Fig. 7A indicates that the amorphous structure is characterized by many undercoordinated Mo atoms. In this situation, load favors the increase of the density of the structure. On the other hand, shear stress generated by sliding is also essential for the formation of tribofilms. During sliding, stick–slip phenomena occur due to the attractive interaction between two adjacent layers, as shown in Appendix. The misplaced atoms are dragged by one of the sliding layers until they find and react with a vacancy, stabilizing the structure. This phenomenon is difficult at first, when the surfaces are highly corrugated and rich in defects. Indeed, sliding is initially quite slow in our simulations in the presence of a high load. At later stages, when surfaces are flatter and defects are mostly disappeared, sliding requires less effort, yet the remaining misplaced atoms might need to travel long distances before encountering a vacancy, slowing down the final steps of the crystallization. This mechanism might explain the slowdown that has been observed experimentally at later stages of the crystallization [49].

In order to counteract the high friction observed at the beginning of the simulations due to the high load, the shear force of the layers or the temperature of the system could be increased. Indeed, several authors demonstrated experimentally that high temperatures improve the crystallinity of the MoS_2 layers [49,55,56]. In our simulations, we found that temperature changes in the range we considered are not sufficient to allow significant mobility of the defects, and higher temperatures should provide significantly different results. On the other hand, increasing the shear force, which indirectly causes the temperature of the system to raise due to energy dissipation, was more helpful than a direct temperature increase.

4. Conclusions

We investigated the transformation of the central core units of MoDTC lubricant additives into an amorphous MoS_x layer and then a crystalline layer of MoS_2 by means of QM/MM and Car–Parrinello simulations. The geometry of the MoS_x units can be significantly transformed in the presence of mechanical stresses. While molybdenum atoms tend to remain in the middle of the amorphous layer, S and O atoms diffuse toward the surfaces of the layer. This geometric rearrangement is an inherent feature of the amorphous layer because it

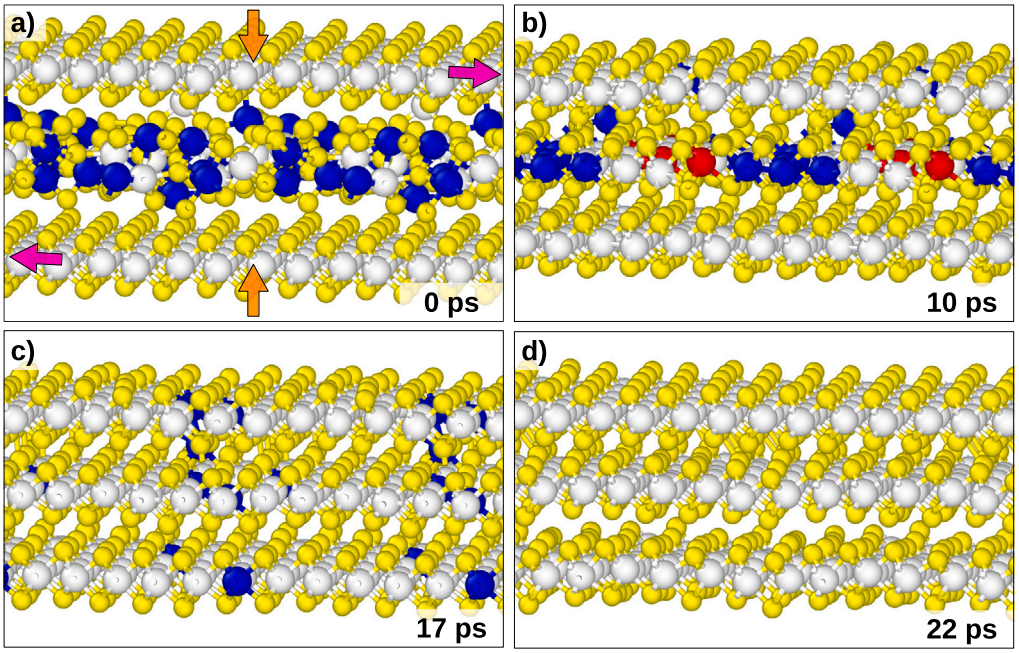

Fig. 7. Snapshots of Simulation 8 at the times indicated in the bottom-right corner of each panel. Orange and purple arrows identify load and shear, respectively, that are present at all times during the simulation. Sulfur atoms are colored in yellow, while molybdenum atoms are colored in blue, white and red depending on whether their coordination number is lower, equal or higher than 6, respectively. The cutoff distance for the neighbor detection was set to 2.6 Å.

Table A.2
Parameters for the attractive and repulsive Lennard-Jones potentials describing the O–S and O–Mo interactions. ϵ and σ are expressed in eV and angstrom, respectively.

	ϵ_{O-S}	σ_{O-S}	ϵ_{O-Mo}	σ_{O-Mo}
Attractive	3.148	0.0197654198	3.683	0.00406400943
Repulsive	0.0002535	4.0264	0.0002535	4.0264

can be achieved in the presence of high loads and independently of the chemical nature of the substrates, as suggested by other authors in previous works. High load are useful to promote bond breaking and forming, while sliding helps misplaced atoms to reach crystalline sites. With this study, we closed the gap in the description of the mechanism that transforms MoDTC additives into MoS_2 tribolayers and proposed an atomistic description of the crystallization process, that can be relevant not only for tribology, but also for several applications unrelated to the study of friction.

CRediT authorship contribution statement

Stefan Peeters: Investigation, Writing – original draft. **Gabriele Losi:** Investigation. **Paolo Restuccia:** Investigation, Writing – review & editing. **M.C. Righi:** Conceptualization, Supervision, Funding acquisition, Writing – review & editing.

Declaration of competing interest

The authors declare that they have no known competing financial interests or personal relationships that could have appeared to influence the work reported in this paper.

Data availability

Data will be made available on request.

Acknowledgments

These results are part of the “Advancing Solid Interface and Lubricants by First Principles Material Design (SLIDE)” project that has received funding from the European Research Council (ERC) under the European Union’s Horizon 2020 research and innovation program (Grant agreement No. 865633). We acknowledge the CINECA award under the ISCRA initiative, for the availability of high performance computing resources and support. The geometries of the systems were visualized and represented in this work using XCrySDen [57], VMD [58] and OVITO [59].

Appendix A. Lennard-Jones potentials

In order to qualitatively describe the interaction between the oxygen atoms in the quantum region and the classical molybdenum and sulfur atoms, Lennard-Jones potentials were employed. The attractive potential was parametrized according to the values reported in literature for Mo, S [60] and O atoms [61] and the values of ϵ for the different species were multiplied by 2 in order to enhance the stability of the Mo–O and S–O interactions. The parameters for both the attractive and repulsive Lennard-Jones potentials for the O–S and O–Mo interactions are reported in Table A.2.

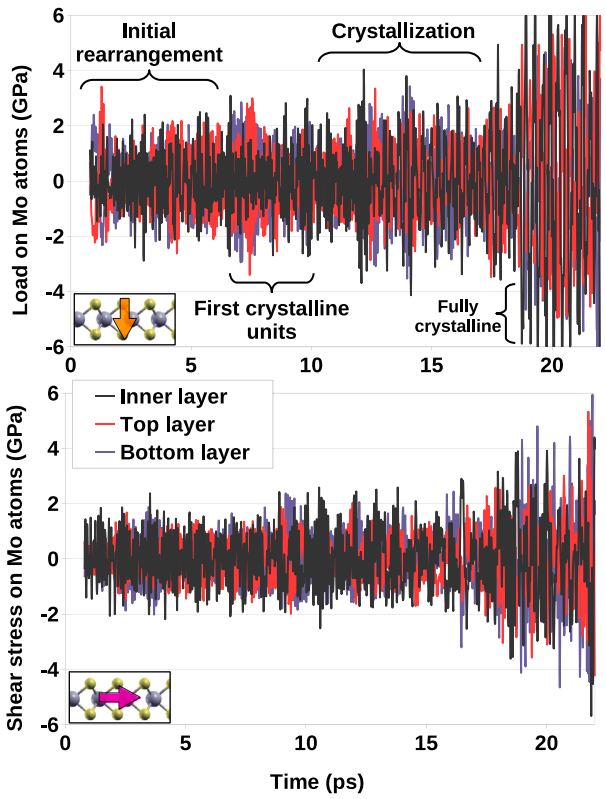

Fig. B.8. Top and bottom: load and shear stress experienced by the Mo atoms of the three layers during Car–Parrinello Simulation 8, respectively. The legend in the middle of the Figure applies to both panels. The insets in the bottom-left corners of the plots represent the force components of the Mo atoms considered for the stress calculation. Different phases of the crystallization are indicated in the top panel.

Appendix B. Stresses on the Mo atoms during the crystallization

Fig. B.8 shows the load and the shear stress experienced by the Mo atoms in Car–Parrinello simulation 8. The load was calculated as:

$$F_N = \frac{1}{A}\sum_i F_i^z \tag{B.1}$$

where A is the area of the simulation cell, F^z is the z-component of the atomic force and the index i runs over all the molybdenum atoms of a specific layer. Similarly, the shear stress τ is obtained by substituting F^z with F^x in the previous equation. These values do not take into account the external forces that are constantly applied to the system, hence the average value of zero for both quantities.

These plots are characterized by high-frequency oscillations due to the stick–slip effect of the sliding layers. Since detecting different phases during the crystallization is not straightforward in these plots, the different regimes are schematically indicated in the figure. The high peaks at the end of the simulations are due to the fact that the sliding speeds up and the external layers start to oscillate in the vertical direction, periodically pushing the inner layer.

References

[1] M.A. Lukowski, A.S. Daniel, F. Meng, A. Forticaux, L. Li, S. Jin, Enhanced hydrogen evolution catalysis from chemically exfoliated metallic mos2 nanosheets, J. Am. Chem. Soc. 135 (2013) 10274–10277, http://dx.doi.org/10.1021/ja404523s, arXiv:http://dx.doi.org/10.1021/ja404523s, pMID: 23790049.

[2] J.D. Benck, T.R. Hellstern, J. Kibsgaard, P. Chakthranont, T.F. Jaramillo, Catalyzing the hydrogen evolution reaction (her) with molybdenum sulfide nanomaterials, ACS Catal. 4 (2014) 3957–3971, http://dx.doi.org/10.1021/cs500923c, arXiv:http://dx.doi.org/10.1021/cs500923c.

[3] Y. Huang, Y. Sun, X. Zheng, T. Aoki, B. Pattengale, J. Huang, X. He, W. Bian, S. Younan, N. Williams, J. Hu, J. Ge, N. Pu, X. Yan, X. Pan, L. Zhang, Y. Wei, J. Gu, Atomically engineering activation sites onto metallic 1t-mos2 catalysts for enhanced electrochemical hydrogen evolution, Nature Commun. 10 (2019) 982, http://dx.doi.org/10.1038/s41467-019-08877-9.

[4] J. Mao, Y. Wang, Z. Zheng, D. Deng, The rise of two-dimensional mos2 for catalysis, Front. Phys. 13 (2018) 138118, http://dx.doi.org/10.1007/s11467-018-0812-0.

[5] Y. Wu, S. Ringe, C.-L. Wu, W. Chen, A. Yang, H. Chen, M. Tang, G. Zhou, H.Y. Hwang, K. Chan, Y. Cui, A two-dimensional mos2 catalysis transistor by solid-state ion gating manipulation and adjustment (sigma), Nano Lett. 19 (2019) 7293–7300, http://dx.doi.org/10.1021/acs.nanolett.9b02888, arXiv:http://dx.doi.org/10.1021/acs.nanolett.9b02888, pMID: 31499003.

[6] B.C. Bayer, R. Kaindl, M. Reza Ahmadpour Monazam, T. Susi, J. Kotakoski, T. Gupta, D. Eder, W. Waldhauser, J.C. Meyer, Atomic-scale in situ observations of crystallization and restructuring processes in two-dimensional mos2 films, ACS Nano 12 (2018) 8758–8769, http://dx.doi.org/10.1021/acsnano.8b04945, arXiv:http://dx.doi.org/10.1021/acsnano.8b04945, pMID: 30075065.

[7] H. Spikes, Friction modifier additives, Tribol. Lett. 60 (2015) 5, http://dx.doi.org/10.1007/s11249-015-0589-z.

[8] T.W. Scharf, S.V. Prasad, Solid lubricants: a review, J. Mater. Sci. 48 (2013) 511–531, http://dx.doi.org/10.1007/s10853-012-7038-2.

[9] Y. Yamamoto, S. Gondo, Friction and wear characteristics of molybdenum dithiocarbamate and molybdenum dithiophosphate, Tribol. Trans. 32 (1989) 251–257, http://dx.doi.org/10.1080/10402008908981886.

[10] Y. Morita, T. Onodera, A. Suzuki, R. Sahnoun, M. Koyama, H. Tsuboi, N. Hatakeyama, A. Endou, H. Takaba, M. Kubo, C.A. Del Carpio, T. Shin-yoshi, N. Nishino, A. Suzuki, A. Miyamoto, Development of a new molecular dynamics method for tribochemical reaction and its application to formation dynamics of mos2 tribofilm, Appl. Surf. Sci. 254 (2008) 7618–7621, http://dx.doi.org/10.1016/j.apsusc.2008.01.123, https://www.sciencedirect.com/science/article/pii/S0169433208001876, 9th International Conference on Atomically Controlled Surfaces, Interfaces and Nanostructures 2007 (ASCIN-9).

[11] Y.-H. Lee, L. Yu, H. Wang, W. Fang, X. Ling, Y. Shi, C.-T. Lin, J.-K. Huang, M.-T. Chang, C.-S. Chang, M. Dresselhaus, T. Palacios, L.-J. Li, J. Kong, Synthesis and transfer of single-layer transition metal disulfides on diverse surfaces, Nano Lett. 13 (2013) 1852–1857, http://dx.doi.org/10.1021/nl400687n, arXiv:http://dx.doi.org/10.1021/nl400687n, pMID: 23506011.

[12] L.P. Hansen, E. Johnson, M. Brorson, S. Helveg, Growth mechanism for single- and multi-layer mos2 nanocrystals, J. Phys. Chem. C 118 (2014) 22768–22773, http://dx.doi.org/10.1021/jp5069279, arXiv:http://dx.doi.org/10.1021/jp5069279.

[13] S.C. Lee, J.D. Benck, C. Tsai, J. Park, A.L. Koh, F. Abild-Pedersen, T.F. Jaramillo, R. Sinclair, Chemical and phase evolution of amorphous molybdenum sulfide catalysts for electrochemical hydrogen production, ACS Nano 10 (2016) 624–632, http://dx.doi.org/10.1021/acsnano.5b05652, arXiv:http://dx.doi.org/10.1021/acsnano.5b05652, pMID: 26624225.

[14] L. Fei, S. Lei, W.-B. Zhang, W. Lu, Z. Lin, C.H. Lam, Y. Chai, Y. Wang, Direct tem observations of growth mechanisms of two-dimensional mos2 flakes, Nature Commun. 7 (2016) 12206, http://dx.doi.org/10.1038/ncomms12206.

[15] W. Tillmann, A. Wittig, D. Stangier, H. Moldenhauer, C.-A. Thomann, J. Debus, D. Aurich, A. Bruemmer, Temperature-dependent tribological behavior of mosx thin films synthesized by hipims, Tribol. Int. 153 (2021) 106655, http://dx.doi.org/10.1016/j.triboint.2020.106655, https://www.sciencedirect.com/science/article/pii/S0301679X20304813.

[16] P. Nicolini, R. Capozza, P. Restuccia, T. Polcar, Structural ordering of molybdenum disulfide studied via reactive molecular dynamics simulations, ACS Appl. Mater. Interfaces 10 (2018) 8937–8946, http://dx.doi.org/10.1021/acsami.7b17960, arXiv:http://dx.doi.org/10.1021/acsami.7b17960.

[17] I. Ponomarev, T. Polcar, P. Nicolini, New reactive force field for simulations of mos2 crystallization, J. Phys. Chem. C 126 (2022) 9475–9481, http://dx.doi.org/10.1021/acs.jpcc.2c01075, arXiv:http://dx.doi.org/10.1021/acs.jpcc.2c01075.

[18] R. Chen, A. Jusufi, A. Schilowitz, A. Martini, Formation of mos2 from elemental mo and s using reactive molecular dynamics simulations, J. Vac. Sci. Technol. A 38 (2020) 022201, http://dx.doi.org/10.1116/1.5128377, arXiv:http://dx.doi.org/10.1116/1.5128377.

[19] S.J. Stuart, A.B. Tutein, J.A. Harrison, A reactive potential for hydrocarbons with intermolecular interactions, J. Chem. Phys. 112 (2000) 6472–6486, http://dx.doi.org/10.1063/1.481208, arXiv:http://dx.doi.org/10.1063/1.481208.

[20] A.C.T. van Duin, S. Dasgupta, F. Lorant, W.A. Goddard, Reaxff: A reactive force field for hydrocarbons, J. Phys. Chem. A 105 (2001) 9396–9409, http://dx.doi.org/10.1021/jp004368u, arXiv:http://dx.doi.org/10.1021/jp004368u.

[21] P. Restuccia, M. Ferrario, M. Righi, Monitoring water and oxygen splitting at graphene edges and folds: Insights into the lubricity of graphitic materials, Carbon 156 (2020) 93–103, http://www.sciencedirect.com/science/article/pii/S0008622319309455, doi=10.1016/j.carbon.2019.09.040.

[22] C. Grossiord, K. Varlot, J.-M. Martin, T.L. Mogne, C. Esnouf, K. Inoue, MoS_2 single sheet lubrication by molybdenum dithiocarbamate, Tribol. Int. 31 (1998) 737–743, http://dx.doi.org/10.1016/S0301-679X(98)00094-2, http://www.sciencedirect.com/science/article/pii/S0301679X98000942.

[23] D.N. Khaemba, A. Neville, A. Morina, New insights on the decomposition mechanism of molybdenum dialkyldithiocarbamate (modtc): A raman spectroscopic study, RSC Adv. 6 (2016) 38637–38646, http://dx.doi.org/10.1039/C6RA00652C.

[24] M. De Feo, C. Minfray, M.I. De Barros Bouchet, B. Thiebaut, J.M. Martin, Modtc friction modifier additive degradation: Correlation between tribological performance and chemical changes, RSC Adv. 5 (2015) 93786–93796, http://dx.doi.org/10.1039/C5RA15250J.

[25] S. Bec, A. Tonck, J.M. Georges, G.W. Roper, Synergistic effects of modtc and zdtp on frictional behaviour of tribofilms at the nanometer scale, Tribol. Lett. 17 (2004) 797–809, http://dx.doi.org/10.1007/s11249-004-8088-7.

[26] A. Somayaji, P.B. Aswath, The role of antioxidants on the oxidation stability of oils with f-zddp and zddp, and chemical structure of tribofilms using xanes, Tribol. T. 52 (2009) 511–525, http://dx.doi.org/10.1080/10402000902745499, arXiv:http://dx.doi.org/10.1080/10402000902745499.

[27] M. Kasrai, J.N. Cutler, K. Gore, G. Canning, G.M. Bancroft, K.H. Tan, The chemistry of antiwear films generated by the combination of zddp and modtc examined by x-ray absorption spectroscopy, Tribol. Trans. 41 (1998) 69–77, http://dx.doi.org/10.1080/10402009808983723.

[28] S. Peeters, P. Restuccia, S. Loehlé, B. Thiebaut, M.C. Righi, Characterization of molybdenum dithiocarbamates by first-principles calculations, J. Phys. Chem. A 123 (2019) 7007–7015, http://dx.doi.org/10.1021/acs.jpca.9b03930, arXiv:http://dx.doi.org/10.1021/acs.jpca.9b03930.

[29] S. Peeters, P. Restuccia, S. Loehlé, B. Thiebaut, M.C. Righi, Tribochemical reactions of modtc lubricant additives with iron by quantum mechanics/molecular mechanics simulations, J. Phys. Chem. C 124 (2020) 13688–13694, http://dx.doi.org/10.1021/acs.jpcc.0c02211, arXiv:http://dx.doi.org/10.1021/acs.jpcc.0c02211.

[30] S. Peeters, C. Charrin, I. Duron, S. Loehlé, B. Thiebaut, M. Righi, Importance of the catalytic effect of the substrate in the functionality of lubricant additives: the case of molybdenum dithiocarbamates, Mater. Today Chem. 21 (2021) 100487, http://dx.doi.org/10.1016/j.mtchem.2021.100487, https://www.sciencedirect.com/science/article/pii/S2468519421000677.

[31] G. Losi, S. Peeters, F. Delayens, H. Vezin, S. Loehlé, B. Thiebaut, M.C. Righi, Experimental and ab initio characterization of mononuclear molybdenum dithiocarbamates in lubricant mixtures, Langmuir 37 (2021) 4836–4846, http://dx.doi.org/10.1021/acs.langmuir.1c00029, arXiv:http://dx.doi.org/10.1021/acs.langmuir.1c00029, pMID: 33847121.

[32] D.N. Khaemba, A. Neville, A. Morina, A methodology for raman characterisation of modtc tribofilms and its application in investigating the influence of surface chemistry on friction performance of modtc lubricants, Tribol. Lett. 59 (2015) 38, http://dx.doi.org/10.1007/s11249-015-0566-6.

[33] D.N. Khaemba, (Ph.D. thesis), University of Leeds, 2016, http://etheses.whiterose.ac.uk/12923/.

[34] A. Warshel, M. Karplus, Calculation of ground and excited state potential surfaces of conjugated molecules. i. formulation and parametrization, J. Am. Chem. Soc. 94 (1972) 5612–5625, http://dx.doi.org/10.1021/ja00771a014.

[35] A. Warshel, M. Levitt, Theoretical studies of enzymic reactions: Dielectric, electrostatic and steric stabilization of the carbonium ion in the reaction of lysozyme, J. Mol. Biol. 103 (1976) 227–249, http://dx.doi.org/10.1016/0022-2836(76)90311-9, http://www.sciencedirect.com/science/article/pii/0022283676903119.

[36] P. Restuccia, M. Ferrario, M.C. Righi, Quantum mechanics/molecular mechanics (qm/mm) applied to tribology: Real-time monitoring of tribochemical reactions of water at graphene edges, Comput. Mater. Sci. (2019) 109400, http://dx.doi.org/10.1016/j.commatsci.2019.109400, http://www.sciencedirect.com/science/article/pii/S0927025619306998.

[37] P.D. Fleischauer, J.R. Lince, A comparison of oxidation and oxygen substitution in mos_2 solid film lubricants, Tribol. Int. 32 (1999) 627–636, http://dx.doi.org/10.1016/S0301-679X(99)00088-2, http://www.sciencedirect.com/science/article/pii/S0301679X99000882.

[38] R. Car, M. Parrinello, Unified approach for molecular dynamics and density-functional theory, Phys. Rev. Lett. 55 (1985) 2471–2474, http://dx.doi.org/10.1103/PhysRevLett.55.2471, https://link.aps.org/doi/10.1103/PhysRevLett.55.2471.

[39] P. Giannozzi, S. Baroni, N. Bonini, M. Calandra, R. Car, C. Cavazzoni, D. Ceresoli, G.L. Chiarotti, M. Cococcioni, I. Dabo, A.D. Corso, S. de Gironcoli, S. Fabris, G. Fratesi, R. Gebauer, U. Gerstmann, C. Gougoussis, A. Kokalj, M. Lazzeri, L. Martin-Samos, N. Marzari, F. Mauri, R. Mazzarello, S. Paolini, A. Pasquarello, L. Paulatto, C. Sbraccia, S. Scandolo, G. Sclauzero, A.P. Seitsonen, A. Smogunov, P. Umari, R.M. Wentzcovitch, Quantum espresso: A modular and open-source software project for quantum simulations of materials, J. Phys. Condens. Matter 21 (2009) 395502, http://stacks.iop.org/0953-8984/21/i=39/a=395502.

[40] J.P. Perdew, K. Burke, M. Ernzerhof, Generalized gradient approximation made simple, Phys. Rev. Lett. 77 (1996) 3865–3868, http://dx.doi.org/10.1103/PhysRevLett.77.3865, https://link.aps.org/doi/10.1103/PhysRevLett.77.3865.

[41] H.M. Senn, W. Thiel, Qm/mm methods for biomolecular systems, Angew. Chem., Int. Ed. 48 (2009) 1198–1229, http://dx.doi.org/10.1002/anie.200802019, https://onlinelibrary.wiley.com/doi/abs/10.1002/anie.200802019, arXiv:https://onlinelibrary.wiley.com/doi/pdf/10.1002/anie.200802019.

[42] S. Plimpton, Fast parallel algorithms for short-range molecular dynamics, J. Comput. Phys. 117 (1995) 1–19, http://dx.doi.org/10.1006/jcph.1995.1039, http://www.sciencedirect.com/science/article/pii/S002199918571039X.

[43] T. Liang, S.R. Phillpot, S.B. Sinnott, Parametrization of a reactive many-body potential for mo-s systems, Phys. Rev. B 79 (2009) 245110, https://link.aps.org/doi/10.1103/PhysRevB.79.245110.

[44] T. Liang, S.R. Phillpot, S.B. Sinnott, Erratum: Parametrization of a reactive many-body potential for mo–s systems [phys. rev. b 79, 245110 (2009)], Phys. Rev. B 85 (2012) 199903, http://dx.doi.org/10.1103/PhysRevB.85.199903, https://link.aps.org/doi/10.1103/PhysRevB.85.199903.

[45] W. Zhang, Z. Huang, W. Zhang, Y. Li, Two-dimensional semiconductors with possible high room temperature mobility, Nano Res. 7 (2014) 1731–1737, http://dx.doi.org/10.1007/s12274-014-0532-x.

[46] G. Zilibotti, S. Corni, M.C. Righi, Load-induced confinement activates diamond lubrication by water, Phys. Rev. Lett. 111 (2013) 146101, http://dx.doi.org/10.1103/PhysRevLett.111.146101.

[47] S. Grimme, Semiempirical gga-type density functional constructed with a long-range dispersion correction, J. Comput. Chem. 27 (2006) 1787–1799, http://dx.doi.org/10.1002/jcc.20495, https://onlinelibrary.wiley.com/doi/abs/10.1002/jcc.20495, http://arxiv.org/abs/https://onlinelibrary.wiley.com/doi/pdf/10.1002/jcc.20495[arXiv:https://onlinelibrary.wiley.com/doi/pdf/10.1002/jcc.20495].

[48] M. Krbal, V. Prokop, A.A. Kononov, J.R. Pereira, J. Mistrik, A.V. Kolobov, P.J. Fons, Y. Saito, S. Hatayama, Y. Shuang, Y. Sutou, S.A. Rozhkov, J.R. Stellhorn, S. Hayakawa, I. Pis, F. Bondino, Amorphous-to-crystal transition in quasi-two-dimensional mos2: Implications for 2d electronic devices, ACS Appl. Nano Mater. 4 (2021) 8834–8844, http://dx.doi.org/10.1021/acsanm.1c01504, arXiv:http://dx.doi.org/10.1021/acsanm.1c01504.

[49] R.A. Vilá, R. Rao, C. Muratore, E. Bianco, J.A. Robinson, B. Maruyama, N.R. Glavin, In situ crystallization kinetics of two-dimensional mos_2, 2D Mater. 5 (2017) 011009, http://dx.doi.org/10.1088/2053-1583/aa9674.

[50] S.-L. Shang, G. Lindwall, Y. Wang, J.M. Redwing, T. Anderson, Z.-K. Liu, Lateral versus vertical growth of two-dimensional layered transition-metal dichalcogenides: Thermodynamic insight into mos2, Nano Lett. 16 (2016) 5742–5750, http://dx.doi.org/10.1021/acs.nanolett.6b02443, arXiv:http://dx.doi.org/10.1021/acs.nanolett.6b02443, pMID: 27540753.

[51] N.N. Gosvami, J.A. Bares, F. Mangolini, A.R. Konicek, D.G. Yablon, R.W. Carpick, Mechanisms of antiwear tribofilm growth revealed in situ by single-asperity sliding contacts, Science 348 (2015) 102–106, http://dx.doi.org/10.1126/science.1258788, https://www.science.org/doi/abs/10.1126/science.1258788, arXiv:https://www.science.org/doi/pdf/10.1126/science.1258788.

[52] S. Raghuraman, P. Boonpuek, K.H. King, Z. Ye, J.R. Felts, The role of speed in atomic scale wear, J. Phys. Chem. C 125 (2021) 4139–4145, http://dx.doi.org/10.1021/acs.jpcc.0c09191, arXiv:http://dx.doi.org/10.1021/acs.jpcc.0c09191.

[53] A. Martini, S.H. Kim, Activation volume in shear-driven chemical reactions, Tribol. Lett. 69 (2021) 150, http://dx.doi.org/10.1007/s11249-021-01522-x.

[54] H. Yu, Z. Zheng, H. Chen, D. Qiao, D. Feng, Z. Gong, G. Dong, An investigation of tribochemical reaction kinetics from the perspective of tribo-oxidation, Tribol. Int. 165 (2022) 107289, http://dx.doi.org/10.1016/j.triboint.2021.107289, https://www.sciencedirect.com/science/article/pii/S0301679X21004370.

[55] H. Zhang, H. Lin, Y. Zheng, Y. Hu, A. MacLennan, Understanding of the effect of synthesis temperature on the crystallization and activity of nano-mos2 catalyst, Appl. Catal. B 165 (2015) 537–546, http://dx.doi.org/10.1016/j.apcatb.2014.10.046, https://www.sciencedirect.com/science/article/pii/S0926337314006663.

[56] B. Kohlhauser, C.I. Vladu, C. Gachot, P.H. Mayrhofer, M. Rodríguez Ripoll, Reactive in-situ formation and self-assembly of mos2 nanoflakes in carbon tribofilms for low friction, Mater. Des. 199 (2021) 109427, http://dx.doi.org/10.1016/j.matdes.2020.109427, https://www.sciencedirect.com/science/article/pii/S0264127520309631.

[57] A. Kokalj, Computer graphics and graphical user interfaces as tools in simulations of matter at the atomic scale, Comput. Mater. Sci. 28 (2003) 155–168, http://dx.doi.org/10.1016/S0927-0256(03)00104-6, http://www.sciencedirect.com/science/article/pii/S0927025603001046, proceedings of the Symposium on Software Development for Process and Materials Design.

[58] W. Humphrey, A. Dalke, K. Schulten, VMD – visual molecular dynamics, J. Mol. Graph. 14 (1996) 33–38.

[59] A. Stukowski, Visualization and analysis of atomistic simulation data with OVITO-the open visualization tool, Modelling Simulation Mater. Sci. Eng. 18 (2010) http://dx.doi.org/10.1088/0965-0393/18/1/015012.

[60] J.A. Stewart, D.E. Spearot, Atomistic simulations of nanoindentation on the basal plane of crystalline molybdenum disulfide (MoS2), Modelling Simulation Mater. Sci. Eng. 21 (2013) 045003, http://dx.doi.org/10.1088/0965-0393/21/4/045003.

[61] H.J.C. Berendsen, J.R. Grigera, T.P. Straatsma, The missing term in effective pair potentials, J. Phys. Chem. 91 (1987) 6269–6271, http://dx.doi.org/10.1021/j100308a038.